The effects of polymer molecular weight on filament thinning and drop breakup in microchannels

2009 New J. Phys. 11 115006

(http://iopscience.iop.org/1367-2630/11/11/115006)

New Journal of Physics
The open-access journal for physics

The effects of polymer molecular weight on filament thinning and drop breakup in microchannels

P E Arratia[1], L-A Cramer[1], J P Gollub[2,3] and D J Durian[2]

[1] Department of Mechanical Engineering and Applied Mechanics, University of Pennsylvania, Philadelphia, PA 19104, USA
[2] Department of Physics and Astronomy, University of Pennsylvania, Philadelphia, PA 19104, USA
[3] Department of Physics and Astronomy, Haverford College, Haverford, PA 19041, USA
E-mail: parratia@seas.upenn.edu

New Journal of Physics **11** (2009) 115006 (18pp)
Received 26 July 2009
Published 4 November 2009
Online at http://www.njp.org/
doi:10.1088/1367-2630/11/11/115006

Abstract. We investigate the effects of fluid elasticity on the dynamics of filament thinning and drop breakup processes in a cross-slot microchannel. Elasticity effects are examined using dilute aqueous polymeric solutions of molecular weight (MW) ranging from 1.5×10^3 to 1.8×10^7. Results for polymeric fluids are compared to those for a viscous Newtonian fluid. The shearing or continuous phase that induces breakup is mineral oil. All fluids possess similar shear-viscosity (~ 0.2 Pa s) so that the viscosity ratio between the oil and aqueous phases is close to unity. Measurements of filament thickness as a function of time show different thinning behavior for the different aqueous fluids. For Newtonian fluids, the thinning process shows a single exponential decay of the filament thickness. For low MW fluids (10^3, 10^4 and 10^5), the thinning process also shows a single exponential decay, but with a decay rate that is slower than for the Newtonian fluid. The decay time increases with polymer MW. For high MW (10^6 and 10^7) fluids, the initial exponential decay crosses over to a second exponential decay in which elastic stresses are important. We show that the decay rate of the filament thickness in this exponential decay regime can be used to measure the steady extensional viscosity of the fluids. At late times, all fluids cross over to an algebraic decay which is driven mainly by surface tension.

Contents

1. Introduction

The progressive breakup of an initially stable fluid thread into a number of small drops is a rich and beautiful phenomenon [1]–[5]. It is also an important dynamical process that impacts many industries including pharmaceutical, petroleum and biotechnology. Recently, there has been a growing interest in microfluidic methods for highly controlled formation of drops [6]–[10] and bubbles [11, 12] that rely on the breakup of fluid threads. A common example is the flow-focusing geometry, which creates drops by focusing a fluid stream into another co-flowing immiscible fluid [6, 12, 13]. In this geometry, the drop size and its distribution are dictated by the relative flow rates of the two fluids. With few exceptions [14]–[16], previous research has been mainly restricted to Newtonian fluids. However, many fluids of interest to lab-on-chip devices are likely to exhibit complex micro-structure and non-Newtonian properties, such as viscoelasticity. In fact, given the small geometrical length scales, one expects viscoelastic behavior to be accentuated in micro-devices. Therefore, understanding the effects of non-Newtonian rheological behavior such as elasticity in micro-devices is of both fundamental and practical importance.

The effects of elasticity on drop breakup have been mainly restricted to macroscopic experiments, in which the outer fluid is typically quiescent [1], [17]–[23]. Usually, the breakup process is driven by capillary pressure, which tends to minimize the interfacial energy of the free surface of a fluid thread by formation of spherical droplets. The necking of the fluid element is resisted by the combined action of viscous and elastic stresses on the fluid thread. This delicate balance of capillary, viscous and elastic stresses gives rise to phenomena that are markedly different from those that occur for Newtonian fluids, including an increase in the fluid thread lifetime and beads-on-string phenomena [24, 25].

The absence of external forcing leads to a necking process that is often self-similar. The evolution of viscoelastic fluid threads undergoing capillary breakup is complex and depends on many factors. In the absence of inertia and in a quiescent bath, it has been shown that the filament diameter (h) undergoes an initial linear viscous thinning, followed by a slower filament thinning in which capillary pressure is balanced by the fluid elastic stresses. In this region, the filament diameter decreases exponentially in time at a rate that is inversely proportional

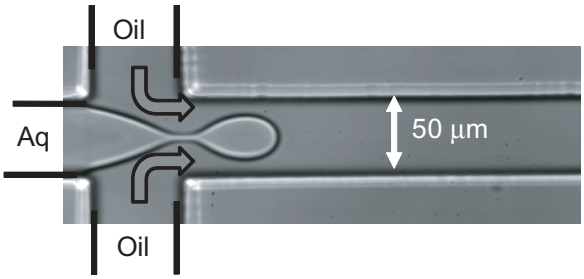

Figure 1. Experimental set-up illustrating the top view of the cross-slot microchannel. The device is molded in PDMS and is 50 μm wide and 50 μm deep. The oil (continuous) phase and the aqueous (dispersed) phase are injected into the device using low-noise syringe pumps.

to the fluid relaxation time $h \sim (1/3\lambda^{-1})$ [26], where λ is the fluid relaxation time. Finally, when polymer molecules become fully extended, the elastic stresses saturate and the filament diameter decreases linearly in time at a rate proportional to σ/η, where σ is the surface tension and η is the viscoelastic fluid viscosity. In the case of viscous Newtonian fluids, the filament thread is predicted to thin linearly in time at a rate proportional to σ/η. The study of this self-thinning process has been used to extract quantitative measures of the fluid material properties in filament stretching and capillary breakup rheometers [20, 27], jet breakup [18], and drop pinch-off [17, 28]. A material property that is often of interest is the fluid extensional viscosity. Most macroscopic investigations provide the transient extensional viscosity of fluids [17, 27, 29]. Here, we provide a method of probing the steady extensional viscosity of fluids.

In this paper, we investigate the effects of polymer molecular weight (MW) on fluid filament thinning and drop breakup in a cross-slot microchannel. Elasticity effects are examined using dilute polymeric solutions of MW ranging from 1.5×10^3 to 1.8×10^7. All polymeric fluids are in the dilute regime, and the elasticity level and values of shear-viscosity are controlled by adjusting the polymer concentration in the fluid. Results for polymeric fluids are compared to those for a viscous Newtonian fluid. We find that the fluid filament thinning process is driven mainly by the outer fluid (oil) viscous stresses. For the Newtonian case, the fluid thins exponentially in time. For low MW fluids (10^3–10^5), the fluid also thins exponentially in time, but at a slower rate, which is dependent on polymer MW. For high MW fluids (10^6–10^7), the thinning process shows two exponential regimes. The first is viscous driven and crosses over into the second regime in which elastic stresses are dominant. We demonstrate that steady extensional viscosity values for the aqueous solutions investigated here can be determined from the exponential thinning regimes.

2. Methods

The experimental configuration is a cross-slot microchannel that is 50 μm wide and 50 μm deep (figure 1). The device is molded in poly(dimethylsiloxane) (PDMS, Dow Sylgard 184) using standard soft-lithography methods [14, 30, 31]. Channels are sealed with a glass cover slip after exposure to an oxygen plasma for 15 s. In order to keep the microchannel wetting properties uniform, the glass cover slip is coated with a thin layer of PDMS prior to the exposure. The assembled channels are then baked for approximately 12 h at 65 °C in order

to obtain hydrophobic walls wetted by the continuous oil phase. The square geometry and channel wetting properties were carefully chosen to minimize three-dimensional effects. Since the flow focusing is in-plane, the filament may not be completely axi-symmetric at its start, but should become more so as it its thickness declines, given the effects of surface tension. It was previously demonstrated that the fluid filament in this geometry is nearly spatially uniform along the channel length, with a thickness that depends only on time [14].

The continuous oil phase is mineral oil containing 0.1% by weight of surfactant (SPAN 80, Fluka). Both Newtonian and polymeric fluids are used for the dispersed aqueous phase. The Newtonian fluid is a 90%-glycerin aqueous solution. Polymeric fluids are made by adding small amounts of the flexible polymer polyacrylamide (PAA, Polysciences, Inc.) to a Newtonian viscous solvent. The level of fluid elasticity is varied by using polymers of different MW. Here we use PAA of MW equal to 1.5×10^3, 1.0×10^4, 9.2×10^4, 1.0×10^6 and 1.8×10^7. We refer to such fluids as 10^3, 10^4, 10^5, 10^6 and 10^7, respectively. The normalized polymer concentration in the viscous solvent is kept constant at $c/c^* = 0.3$ for all fluids, where c^* is the overlap concentration, in order to keep the fluids in the dilute regime. The overlap concentration c^* is proportional to the molecule's radius of gyration ($c^* \propto R_g^{-3}$), and is a function of polymer MW [32, 33]. The values of c^* for the 10^3, 10^4, 10^5, 10^6 and 10^7 fluids are 4.5×10^5, 1.0×10^5, 2.24×10^4, 3.4×10^3 and 350 ppm, respectively. We note that, although polymer chain entanglement is unlikely in this dilute regime, hydrodynamic interactions are possible [34].

The interfacial tension σ between the continuous (mineral oil) and all aqueous phases (Newtonian and polymeric fluids) is approximately $10\,\mathrm{mN\,m^{-1}}$. Results from our experiments, not shown in this paper, show that the morphology and dynamics of the breakup process is not significantly altered for surfactant concentration in the oil phase (C_s) in the range of $0.5\,\mathrm{CMC} < C_s < 5\,\mathrm{CMC}$, where CMC is the critical micelle concentration. For surfactant concentration above 5 CMC, the fluid filament becomes more rigid and long filaments are observed even for the Newtonian case.

All fluids are characterized using a stress-controlled rheometer. In figure 2, we show both the shear-viscosity (η_s) and the measured first normal stress difference (N1) for all fluids as a function of shear rate ($\dot{\gamma}$). The shear viscosities of the oil and Newtonian fluids are nearly identical and independent of shear rate: $\eta_s \approx 0.23\,\mathrm{Pa\,s}$. Since the polymeric fluids are in the dilute regime, the values of η_s are also nearly independent of shear strain-rate: $\eta_s \approx 0.23\,\mathrm{Pa\,s}$. The polymeric fluids, however, display nonzero values of the first normal stress difference (N1), which increases with shear rate. The nonzero values of N1 indicate that the polymeric fluids possess elasticity. Viscoelastic fluids possessing nearly constant viscosity are usually called 'Boger' fluids [35, 36]. They are frequently used to investigate the effects of elasticity on flow behavior since shear-thinning effects are minimized. The choice of fluids also ensures that the viscosity ratio between the oil and aqueous phases (both Newtonian and polymeric) is kept close to unity.

The polymeric fluid shear rheology data is fitted to the widely used finite extensibility nonlinear elastic model with Peterlin's closure (FENE-P) [27, 32, 37]. In this model the fluid total stress tensor τ is assumed to be the sum of a contribution from the solvent and another resulting from the presence of polymer molecules such that $\tau = \tau_{\mathrm{Poly}} + \tau_{\mathrm{Solv}}$. The polymeric fluid shear viscosity η_S is then the sum of polymeric and solvent parts $\eta_s = \eta_{\mathrm{Poly}} + \eta_{\mathrm{Solv}}$. The FENE-P model is well-adapted for dilute (and semidilute) polymeric solutions, and has been used previously to analyze filament thinning of polymeric fluids in macroscopic experiments [23, 28].

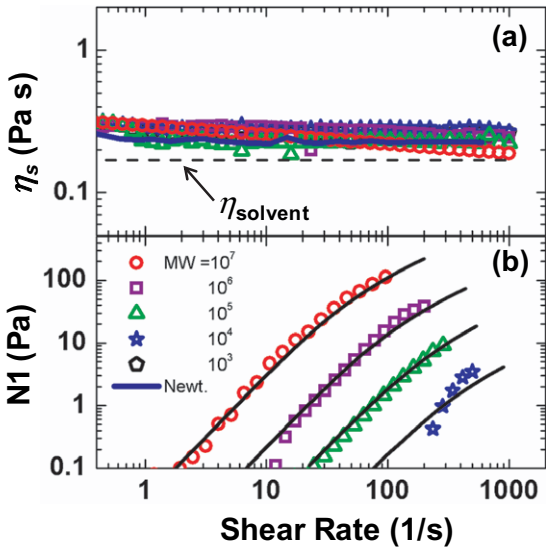

Figure 2. Fluid rheological characterization. (a) Shear viscosity versus shear strain-rate for all fluids. The values of shear viscosities η_s are nearly constant for all fluids. Also shown is the solvent viscosity (dashed line). (b) First normal stress difference (N1) as a function of shear strain-rate for polymeric fluids. Solid lines correspond to a FENE-P model fit [28, 33]. Note that the 10^3 fluid has negligible (measured) values of N1, and it is not shown in (b).

A fluid described by the FENE-P model possesses the same dynamical properties as a fluid described by the much simpler Oldroyd-b model, which assumes that polymers can be modeled as Hookean springs. The main difference is that the Oldroyd-b model allows for infinite extension of polymer molecules, while the FENE-P model uses a spring-force law in which the polymer molecules can be stretched only by a finite amount in the flow field [32, 37].

We perform a simultaneous fit (figure 2) of the polymeric fluid η_S and N1 data to the FENE-P model. The simultaneous fit provides the fluid relaxation time λ and a dimensionless finite extensibility parameter b, which are the only two adjustable parameters [28, 32]. We find that the best fit results for the values of λ are 0.45, 0.06, 0.023 and 0.009 s for the 10^7, 10^6, 10^5 and 10^4 MW fluids, respectively (figure 3(a)). The values of b for all the polymeric fluids are of the order of $O(10^3)$, which is consistent with the literature [28, 33, 38] (figure 3(b)); the minimum fitted values of b is 1000 ($\mathrm{MW} = 10^3$), and the maximum is 4500 ($\mathrm{MW} = 10^7$). The measured values of N1 show an approximately second order dependence on shear-rate ($\mathrm{N1} \propto \dot{\gamma}^2$), which is typical of Boger fluids [35]. Note that due to the rheometer capabilities, we were unable to measure N1 for the 10^3 MW fluid. The relaxation time of the 10^3 MW fluid is estimated to be 9×10^{-4} s by extrapolating λ as a function of MW (figure 3). Note that the extrapolation follows the FENE-P scaling of $\lambda \sim \mathrm{MW}^{2/3}$. Further details on the equations and methods used to fit the FENE-P model to the shear rheology can be found elsewhere [14, 28].

The oil and aqueous phases are injected into the central and side arms of the cross-channel, respectively, using syringe pumps (Harvard Instruments). Experiments are performed for flow rate ratios, $q = Q_{\mathrm{oil}}/Q_{\mathrm{aq}}$, ranging from 10 to 100. In all cases, the aqueous flow rate is kept constant at $Q_{\mathrm{aq}} = 0.01\ \mu\mathrm{l\,min}^{-1}$. This is low enough that the behavior is quasi-static, such that

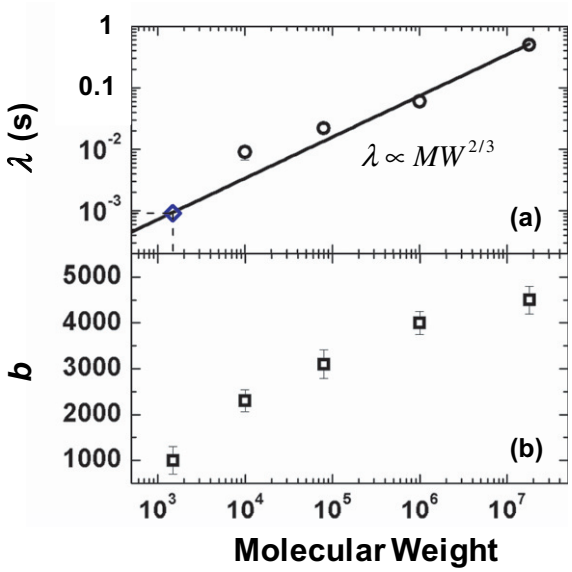

Figure 3. (a) Fluid relaxation times (λ) of polymeric fluids obtained from the FENE-P model fits to the data (circles). The estimated value of λ for the 10^3 polymeric fluid (diamond) is obtained from extrapolating data using a fit (solid line) to λ versus MW data. Note that the fit is consistent with FENE-P scaling $\lambda \propto \mathrm{MW}^{2/3}$. (b) Values of dimensionless finite extensibility parameter b as a function of polymer MW.

the periodicity—but not the morphology—depends on Q_{aq}. For this range of parameters, the Reynolds number is less than 0.01; therefore viscous forces are much larger than inertial forces. Similarly the capillary number ranges from 1.25 to 50; therefore, viscous forces are also larger than surface forces. Under these conditions an aqueous filament is formed and stretched by the flow of the surrounding oil. The thinning and breakup of the filament are imaged using an inverted microscope and a fast video camera, with frame rates between 1 and 10 kHz.

3. Results

3.1. Qualitative observations

In figure 4, we show sample snapshots of the evolution of the filament thinning and drop breakup process for the Newtonian fluid and the polymeric, viscoelastic fluids of different MWs at flow rate ratio $q = 30$. The Newtonian fluid is shown in the leftmost panel. Initially, the aqueous phase is drawn into the cross-slot channel, as shown in figure 4(a). The continuous phase (oil) then begins to elongate the fluid filament (at time $0.15t_{\mathrm{b}}$). Here, t_{b} is the breakup time, which for the Newtonian fluid is 11.5 ms. Also, time zero ($t = 0$) is defined when negative curvature first occurs in the 'mother drop'. The fluid filament collapses and forms a primary drop connected to a very thin filament ($0.45t_{\mathrm{b}}$ and $0.95t_{\mathrm{b}}$); later ($t > t_{\mathrm{b}}$) the filament thins at a faster rate and breaks into a large primary drop and small satellite droplets.

The low MW fluid (10^4) shows very similar qualitative behavior to the Newtonian fluid. One of the main differences, however, is the relatively long and thin fluid filament that connects

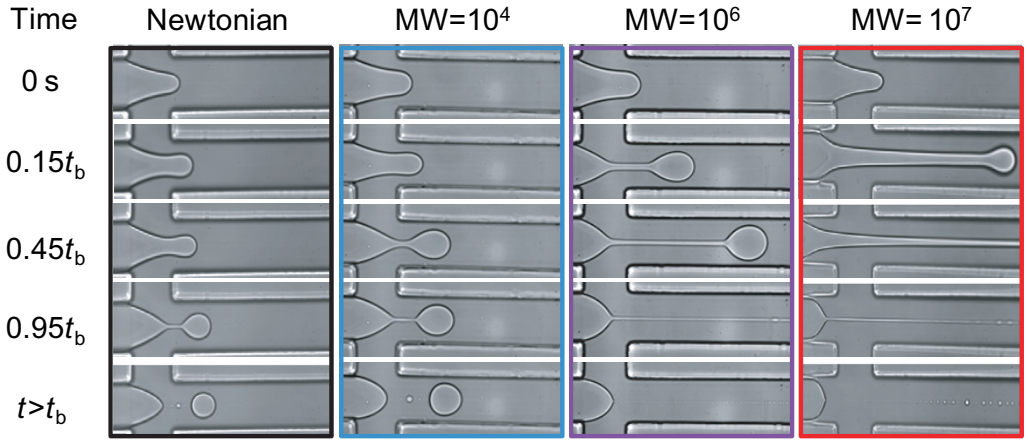

Figure 4. Evolution of the thinning process for a Newtonian fluid (left) and polymeric fluids with MWs equal to 10^4, 10^6 and 10^7 (from left to right) for a flow rate ratio $q = Q_{oil}/Q_{aq} = 30$. Here Q_{oil}/Q_{aq} corresponds to the ratio of oil and aqueous phase flow rates. Mineral oil is the continuous phase while the aqueous phase is either a Newtonian or polymeric fluid. The breakup times (t_b) for the Newtonian and polymeric cases are 11.5, 43.94, 174 and 275 ms, from left to right. The fluid filament becomes longer as the polymer MW is increased. Also, we observe the appearance of satellite droplets in the Newtonian case and multiple beads attached to the filament in the high MW polymeric cases near the breakup event.

the primary drop to the aqueous phase ($0.45t_b$ and $0.95t_b$). The breakup time for this case is 43.94 ms. Similar to the Newtonian fluid, the filament breaks into a large drop and small satellite droplets ($t > t_b$).

The high MW fluids (10^6 and 10^7) display very different behavior. Initially, we observe a morphology that is similar to that of the Newtonian fluid, which indicates that viscoelasticity is negligible at first. As the thinning progresses, the elastic stress builds up and opposes the thinning of the fluid filament ($0.15t_b$). Later, the high MW fluids develop longer necks with a drop attached to it ($0.15t_b$ and $0.45t_b$). This filament elongates while thinning at a much slower rate than in the Newtonian case ($0.45t_b$); the breakup times are 174 and 275 ms for the 10^6 and 10^7 fluids, respectively. Near the breakup event, the polymeric fluid shows multiple beads ('beads-on-string') attached to the filament ($0.95t_b$) [1, 20, 24, 25, 39]. After breakup, there are many small satellite drops.

3.2. Quantifying filament thinning

The filament thinning process is quantified by the decrease in filament thickness $h(t)$ as a function of time. To accomplish this, we fit a third-order polynomial equation to the interface contour, which is restricted to the cross-slot region. The measurement location varies with the fluid, but it is usually confined to the cross-slot region. Also, it was previously found that the exact measurement location has little impact on the overall $h(t)$ data [14]. We assume that the interface is symmetric across the centerline and only half of the contour is fitted with the polynomial. We then locate the absolute value of the minimum in the polynomial first derivative,

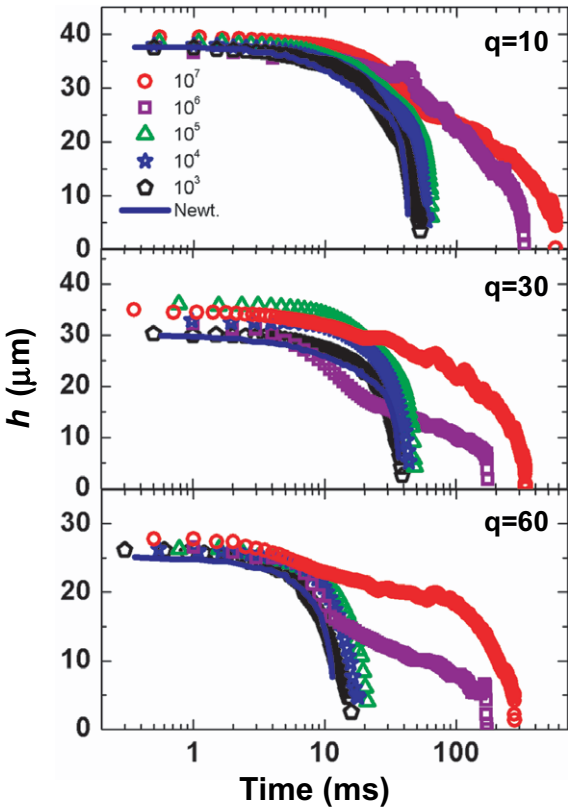

Figure 5. Filament thickness $h(t)$ as a function of time for all polymeric (symbols) and Newtonian fluids (solid line) at different flow rate ratio $q = Q_{\text{oil}}/Q_{\text{aq}}$, where $Q_{\text{aq}} = 0.01\,\mu\text{l}\,\text{min}^{-1}$. Initially, for all fluids and q, the values of $h(t)$ are nearly identical since all fluids have similar values of shear-viscosity. For low MW fluids (10^3, 10^4 and 10^5), the filament thickness decays in a similar fashion to the Newtonian fluid but at a slower rate; the rate decreases as the MW increases. For high MW fluids (10^6 and 10^7), the filament thickness crosses over to a second decay regime, in which elastic stresses are dominant.

which is usually located at the right edge of the field of view, within the cross-slot region. The filament diameter is measured at the point where the absolute value of the minimum in the first derivative is located. Accordingly, the initial time for measurement is set to $t = 0$ when the fitted polynomial second derivative changes sign. Here, we assume that the thinning process is spatially uniform, with a thickness that depends only on time. This assumption was previously tested and proved to be a reasonable one [14].

Sample measurements of filament thickness $h(t)$ as a function of time are presented in figure 5. Results are shown for Newtonian and all polymeric fluids for three flow rate ratios, $q = 10$, 30, and 60. At short times, the Newtonian and all polymeric fluids exhibit identical initial thinning. This behavior is indicative of their similar values of shear-viscosity η_s (figure 2). As time progresses, however, the polymeric fluids begin to diverge from the Newtonian fluid case. For low MW fluids (10^3, 10^4 and 10^5), the fluid thins exponentially but at a slower rate than the Newtonian fluid. As expected, the decay rate decreases as the fluid MW increases, or as the elastic stress increases. For high MW fluids (10^6 and 10^7), the thinning process crosses

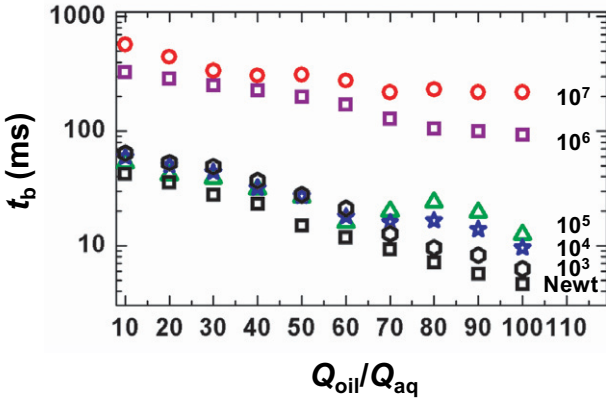

Figure 6. Breakup time as a function of flow rate ratio. Results show an approximately exponential dependence of breakup time on the continuous (oil) viscous stress. The breakup time increases as the polymer MW increases. Note that Q_{aq} is constant at 0.01 μl min^{-1}; thus the breakup time is only a function of Q_{oil} or the outer viscous stress.

over to a second exponential decay, in which the elastic stress is dominant. The duration of this second exponential decay increases with MW. The filament thinning data show that the breakup time (t_b) increases with polymer MW and decreases with flow rate ratio q.

Values of breakup time t_b for all fluids as a function of flow rate ratio q are shown in figure 6. A common feature for all fluids is that the values of t_b display an approximately exponential dependence on q. A similar trend is found in flow-focusing experiments [6, 9] and in a numerical investigation [40]–[42] using Newtonian fluids. The breakup times are longer for the polymeric fluids and increase as the MW increases, even though all polymeric fluids possess the same shear viscosity. For high MW fluids, the breakup time can be an order of magnitude longer than for the Newtonian fluid at a given value of q. This result indicates that the elastic stress has a stabilizing effect on the fluid filament. Moreover, it suggests that the thinning process may be governed by a delicate balance between the outer fluid (oil) viscous stress and the inner fluid visco-elastic stress.

Here, the filament extensional strain-rate is defined as $\dot{\varepsilon} = -(2/h)\mathrm{d}h/\mathrm{d}t$ [14, 17, 25, 29], where h is the filament thickness. The values of $h(t)$ and $\dot{\varepsilon}$ are shown as a function of time for all fluids at $q = 10$ in figures 7(a) and (b), respectively. For the Newtonian fluid, $\dot{\varepsilon}$ is initially independent of time; therefore, in this regime, $h(t)$ decreases exponentially with time. For low MW fluids (10^3, 10^4 and 10^5), the values of $\dot{\varepsilon}$ are also independent of time and quite close to the Newtonian case. However, $\dot{\varepsilon}$ starts deviating from the Newtonian fluid case as time passes. For high MW fluids (10^6 and 10^7), $\dot{\varepsilon}$ is initially equal to the same constant as for the Newtonian fluid. But it soon departs and, after a transient interval, settles down to smaller constant value, which indicates a second regime of slower exponential thinning. For all fluids at the very latest times, close to breakup, the final decrease of $h(t)$ to zero gives an apparent divergence of $\dot{\varepsilon}$. We show later that the data just before breakup are consistent with a linear decrease in filament diameter, $h(t) \propto (t - t_b)$, where t_b is the breakup time.

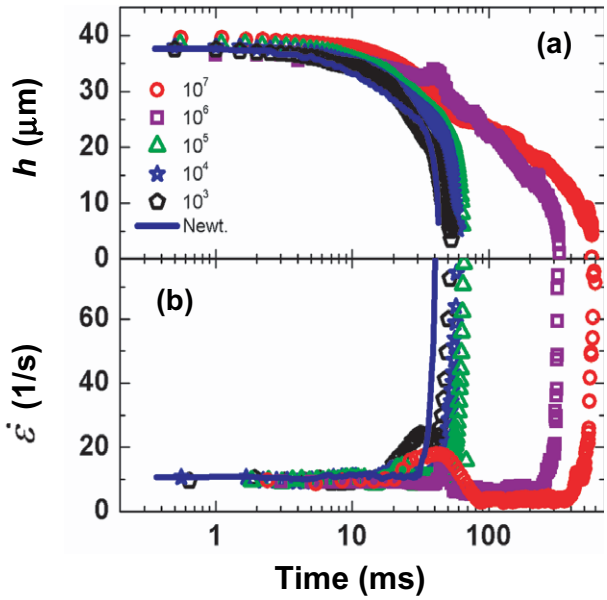

Figure 7. Time dependent filament thinning and corresponding filament strain-rate at flow rate ratio $q = 10$. (a) Filament thickness diameter as a function of time for all polymeric fluids (symbols) and Newtonian fluids (solid line). (b) Extensional strain-rate $\dot{\varepsilon} = -(2/h)\,\mathrm{d}h/\mathrm{d}t$ as a function of time for the same fluids at $q = 10$. The exponential (or extensional) regimes are characterized by constant values of $\dot{\varepsilon}$.

3.3. A simple model

3.3.1. Flow-driven regime. The filament thinning process is modeled by using a simple normal stress balance in the cross-slot region. The main assumption in this model are that (i) filament thinning is driven mainly by the outer fluid (oil) extensional flow in the cross-slot region and (ii) the shear flow that develops is relatively far downstream from the cross-slot region and should have no implications for the local stress balance. These are reasonable assumptions since shear stresses tangential to the filament do not contribute to the thinning (or squeezing) of the filament. In the cross-slot region, the filament thinning is driven by viscous stresses normal to the filament.

We start from the assumption of stress balance inside and outside the interface such that $\eta_e\dot{\varepsilon} = \eta_{e,oil}\dot{\varepsilon}_{oil}$, where the subscript 'oil' is used to label the extensional strain rate and viscosity of the oil phase. This balance relates the extensional strain-rates and extensional viscosities of the aqueous (Newtonian and polymeric fluids) and oil phases. The left and right sides of the stress balance are the extensional viscosity multiplied by the extensional strain-rate for the aqueous filament and continuous oil phases, respectively. Since the oil is a Newtonian fluid, we apply the definition of extensional viscosity so that $\eta_{e,oil} = 3\eta_{s,oil}$ [27, 32, 43]. As mentioned before, the fluid filament strain-rate is defined as $\dot{\varepsilon} = -(2/h)\,\mathrm{d}h/\mathrm{d}t$. The strain-rate for oil in the cross-slot region is $\dot{\varepsilon}_{oil} \approx Q_{oil}/(W^2L)$, as verified by particle-tracking methods [14, 44]. Assuming that η_e is independent of time, then the filament diameter thins according to

$$h(t) = h_0 \exp\left[-(3/2)(\eta_{s,oil}/\eta_e)\dot{\varepsilon}_{oil}t\right]. \tag{1}$$

In the above equation, h_0 is an integration constant. This equation is valid for the two flow-driven exponential regimes shown in figures 5 and 7. In such flow-driven regimes, equation (1) may be used to deduce the values of η_e from $h(t)$ data in regions where the filament strain-rate is constant.

We note that the quantity $\dot{\varepsilon}_{oil} \approx Q_{oil}/(W^2L)$ is measured in the cross-slot region, where the flow is extensional and where pinching from the 'mother drop' occurs. To this end, we have checked that $\dot{\varepsilon}_{oil}$ remains constant during the filament thinning and breakup event; the average velocity of the oil in the cross-slot region is constant since Q_{oil} is kept constant.

3.3.2. Capillary-driven regime. Near the final breakup, capillary forces become important. We model this regime by incorporating the surface tension effects into the normal stress balance. We note that near the breakup, the Rayleigh–Plateau instability sets in, causing beading and the eventual breakup of the fluid thread. Equating radial stresses with the Laplace pressure gives $\eta_e\dot{\varepsilon} = \sigma/h$ [8, 41, 45]. Therefore, the fluid filament is predicted to thin linearly with time according to

$$h(t) = -(1/2)(\sigma/\eta_e)(t - t_b), \tag{2}$$

where t_b is the breakup time. Equation (2) indicates that, near the breakup or singularity, the fluid filament varies linearly with $(t - t_b)$ with a slope or velocity proportional to $\sigma/2\eta_e$, as we find experimentally [14]. A similar result has been obtained numerically [46] in the Stokes regime, except that shear rather than extensional viscosity is used in the denominator. A linear regime is also predicted numerically for polymeric solutions near the breakup regime [26, 47].

Equation (2) provides an alternative method to obtain values of extensional viscosity of the aqueous solutions near the breakup event. In fact, it has been demonstrated [14] that the values of η_e obtained from equation (2) are similar to the values of η_e obtained using equation (1), which is valid in the flow-driven regime. This similarity in η_e values demonstrates the consistency of our extensional viscosity results in the flow- and capillary-driven regimes. We caution, however, that extracting values of η_e near the breakup event is subject to larger statistical errors than in the flow-driven regime because the dynamic range is limited; the imaging resolution is about $2\,\mu$m.

Finally, we note that a different model of the capillary effects is to assume that the fluid thinning is controlled by the rate at which the aqueous solution escapes from the end of the fluid filament. In this argument, the capillary pressure difference between the center of the filament and the end is not a local quantity. However, an equation of the form of equation (2) is still found, but with a different pre-factor [48]. In the experiments performed here, the filament diameter is measured locally (at one point), so an argument based on force balance and mass conservation argument seems appropriate.

3.4. Extensional viscosity

The transition between the two exponential thinning regimes for high MW polymeric fluids can be elucidated by plotting the quantity $\varphi = \dot{\varepsilon}_{oil}\eta_{e,oil}/\dot{\varepsilon}$, which has units of viscosity, as a function of time. In figure 8, we display the quantity φ at different flow rate ratios for the 10^7 MW polymeric fluid. We find that φ is nearly constant in regions where $\dot{\varepsilon}$ is constant. In such regions, the quantity φ is the same as the filament extensional viscosity η_e. Initially, the

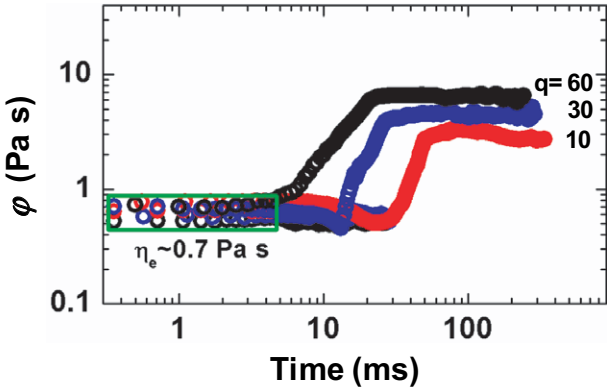

Figure 8. Extensional viscosity versus time for the 10^7 MW fluid at different flow rate ratios q. The quantity $\varphi = \dot{\varepsilon}_{\text{oil}}\eta_{\text{e,oil}}/\dot{\varepsilon}$ is equivalent to the filament extensional viscosity η_{e}, where the flow is extensional, i.e. $\dot{\varepsilon} =$ constant. Here, $\dot{\varepsilon}_{\text{oil}}$ and $\eta_{\text{e,oil}}$ are the oil extensional strain rate and extensional viscosity, respectively. Initially, for all fluids, the values of φ are similar since all fluids have nearly the same η_{s}. Later, the steady-state value of φ increases with larger values of q.

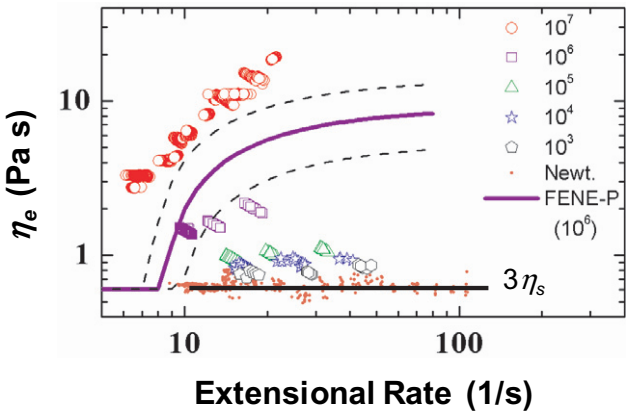

Figure 9. Steady extensional viscosity η_{e} versus extensional strain-rate $\dot{\varepsilon}$ for all fluids. The values of η_{e} are derived from equation (1). The theoretical Trouton ratio for the Newtonian fluid is nearly 3.0 (points), as expected. The polymeric fluids extensional viscosity shows the typical strain-rate hardening behavior. The transition to strain-rate hardening behavior sets in later and the values of η_{e} increase as the polymer MW increases. Also shown is the FENE-P prediction for the 10^6 MW fluid (solid line). The accompanying dashed lines correspond to the uncertainties in measuring λ and b. The FENE-P model is only in qualitative agreement with the measurements.

values of φ are approximately $3\eta_{\text{s}}$ for $q = 10$, 30 and 60 indicating that initially, elastic stresses are not important. After a transient regime, the values of φ are again steady, but larger than the initial values, indicating that elastic stresses have become dominant; φ also depends on q.

In figure 9, we plot the values of extensional viscosity η_{e} for all aqueous solutions, Newtonian and polymeric fluids, as a function of the filament strain-rate $\dot{\varepsilon} = -(2/h)\,\mathrm{d}h/\mathrm{d}t$,

using equation (1). For the Newtonian fluid, the values of η_e are independent of extensional strain-rate. Moreover, we find that the values of η_e are very close to the expected values of $3\eta_s$ [27, 32, 43].

A significantly different behavior is observed for the polymeric fluids. We find that all polymeric fluids show 'strain-rate hardening' behavior. This increase in η_e as function of extensional strain-rate is attributed to the stretching of the polymer molecules in the extensional flow within the thinning filament. This 'strain-rate hardening' behavior has been observed in other macroscopic experiments [17, 25, 29].

It important to point out that the values presented in figure 9 are for *steady* extensional viscosity and not *transient* extensional viscosity, which is usually reported in macroscopic experiments [17], [27]–[29]. Here, values of η_e are computed for each steady extensional strain-rate $\dot{\varepsilon}$, which is proportional to q. In macroscopic experiments, the values of asymptotic η_e are measured when polymer chains are fully stretched, while here the asymptotic η_e gives the degree of extension of polymer chains in the fluid filament for a given value of $\dot{\varepsilon}$.

In figure 9, the corresponding prediction using the FENE-P model is plotted for the 10^6 MW fluid; the accompanying dashed lines correspond to the uncertainties in measuring the parameters λ and b (figure 3). An expression for η_e can be obtained from the FENE-P model for a range of extensional strain-rates [28, 32]. The FENE-P model captures the main qualitative features of η_e such as the 'strain-rate hardening' behavior and the saturation at high values of $\dot{\varepsilon}$. However, there are discrepancies between the model and the estimated values. For high MW, the predicted strain-rate hardening behavior sets in too soon and too abruptly. For low MW fluids, the predicted strain-rate hardening behavior sets in too late (not shown). There are several reasons for these discrepancies including poly dispersion in polymer MW. There are also inherent limitations of the FENE-P model such as the averaging of the force values connecting the beads in the dumb-bell model originally proposed by Peterlin [37]. This averaging is known to lead to unexpectedly large polymeric stresses compared to the non-averaged FENE model [49]. Another limitation is that while real polymeric fluids have a spectrum of fluid relaxation times λ, the FENE-P model, as used here, is described by a mean λ obtained in a shear flow, which is known to be low for use in extensional flows. Therefore, we should expect some type of failure of predictions of η_e based on the single mode FENE-P model. This disagreement, however, does not imply a weakness in the measurement.

3.5. Accumulated strain

Results shown so far suggest that elastic stresses become dominant as the accumulated strain is increased. Here, the accumulated strain experienced by the fluid filament is given by $\varepsilon = \int_0^t \dot{\varepsilon}(t)\,\mathrm{d}t = \int_0^t 2/h(\mathrm{d}h/\mathrm{d}t)\,\mathrm{d}t = 2\ln(h_0/h)$ [27, 29], where $\dot{\varepsilon} = -(2/h)\,\mathrm{d}h/\mathrm{d}t$ and h_0 is the initial value of the filament thickness. A critical (accumulated) strain ε_c is defined at a point in the thinning process at which the elastic stress becomes dominant, and the filament thickness $h(t)$ begins to deviate from the Newtonian behavior. A critical filament thickness h_c is chosen at the first inflection point of h versus time, which yields a critical time t_c. Hence, a critical strain can be defined as

$$\varepsilon_c = \int_0^{t_{cc}} 2/h(\mathrm{d}h/\mathrm{d}t)\,\mathrm{d}t = 2\ln(h_0/h_c). \tag{3}$$

Values of critical strain ε_c are shown in figure 10 for all polymeric fluids for flow rate ratios $q = 10$, 30 and 60. While there is scatter in the data due to the accuracy to which h_c is estimated,

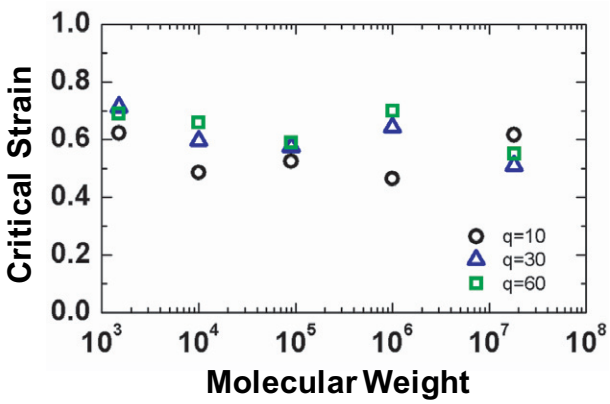

Figure 10. Values of critical strain estimated using equation (3) (see text) for all fluids at $q = Q_{\text{oil}}/Q_{\text{aq}} = 10$, 30 and 60. Within experimental error, the values of accumulated strain are similar for all fluids and q.

a single value of accumulated strain is found. This value of the critical strain is approximately 0.6 for all polymeric fluids at different forcing values (q). This critical strain value is an order of magnitude smaller than the values reported in macroscopic experiments [27, 29]. This lower value of strain suggests that, in addition to flow forcing, both the geometry and system length-scale play an important role in the thinning and breakup process [16].

3.6. Phase diagram

A phase diagram showing all the thinning and breakup regimes found in this investigation is shown in figure 11 as a function of the flow rate ratio $q = Q_{\text{oil}}/Q_{\text{aq}}$, where Q_{aq} is constant, as mentioned in the methods section. The Newtonian fluid is shown in the leftmost part of the x-axis. We find three main regimes as q is increased: slugging, dripping, and streaming. Slugging is found for $q < 25$, while tip-streaming is found for $q > 150$. Dripping is found for $25 < q < 150$.

For high MW fluids (10^6 and 10^7), we find a stable filament that does not exhibit breakup at $q < 15$ (figure 11; inset image in low right corner). As q is increased, the dripping regime sets in and long filaments are observed (figure 11; inset image in mid right corner). At high values of q ($q > 150$), a streaming regime is found in which a sharp tip is formed at the edge of the mother drop that continuously ejects very small droplets (figure 11; inset image in up right corner). This streaming regime is controlled by both elastic stresses and excess surfactant in the 'mother-drop' tip. However, unlike the Newtonian case, the mother drop forms a long fluid filament that extends far beyond the field of view. This fluid filament advances and recoils while ejecting small droplets. To the best of our knowledge, this is the first time that such 'elastic tip-streaming' has been reported in the literature.

As the polymer MW is decreased, the fluid filaments become shorter and the 'streaming' regime is lost. Only dripping and slugging are observed for the low MW fluids (10^3, 10^4 and 10^5) for the flow rate ratios investigated here.

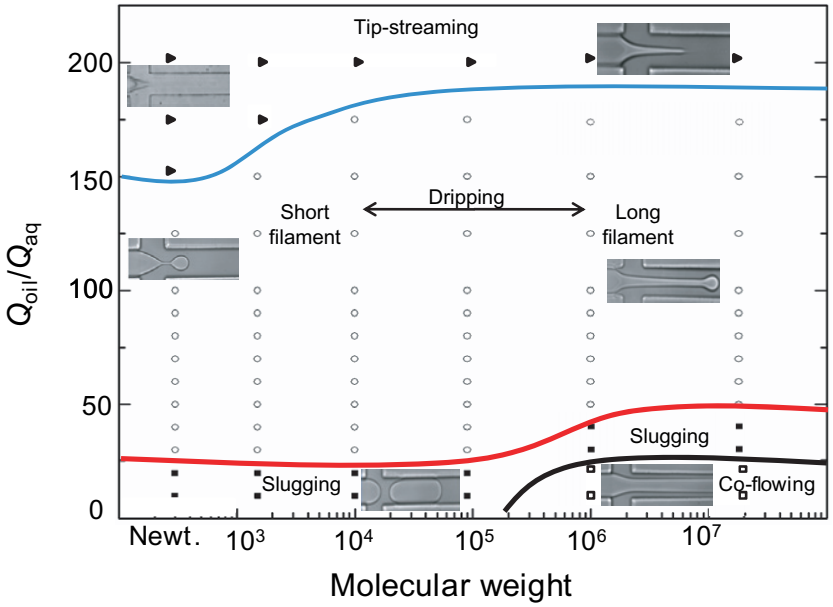

Figure 11. Phase diagram for all fluids at different flow rate ratios $q = Q_{oil}/Q_{aq}$, where $Q_{aq} = 0.01\,\mu l\,min^{-1}$. Three main regimes are found: slugging, dripping and streaming. In addition, a stable filament that does not breakup is found for high MW fluids at low values of q. Tip-streaming is observed at high values of $q > 150$ for Newtonian fluids. Elastic-streaming is observed for high MW fluids and high values of q. No streaming is observed for the low MW fluids at the flow rate ratios investigated here. Dripping is observed at moderate values of q for all fluids.

4. Conclusions

In this paper, we present an experimental investigation of the effects of elastic stresses on the filament thinning and drop breakup processes in a cross-flow microchannel. The elastic stresses are controlled by varying the MWs of a flexible polymer dissolved in a viscous solvent. The polymer MW is varied from 1.5×10^3 to 1.8×10^7 corresponding to fluid relaxation times λ from 9.0×10^{-4} to 0.5 s. Results show that polymeric fluids have a much longer filament than Newtonian fluids of similar shear-viscosity. The fluid filament becomes longer, and the breakup time increases as the MW is increased. Also, near breakup, the polymeric fluids show 'beads-on-string' phenomena.

Measurements of filament thickness (h) as a function of time show two different regimes: flow- and capillary-driven. The flow-driven regime is the main regime in which the fluid filament thins. The capillary-driven regime sets in at a much later time, is short-lived, and is responsible for filament breakup. In the flow driven regime, for Newtonian fluids, the filament thinning process shows a single flow-driven, exponential decay. For low MW fluids (10^3–10^5), the thinning process is also exponential, but with a decay rate that is slower than for the purely viscous Newtonian fluid. The slower exponential decay rate is associated with small, but finite elastic stress. For high MW fluids (10^6–10^7), the thinning crosses over from a initial exponential decay to a second exponential decay in which elastic stress inside the fluid filament becomes dominant.

At late times, all fluids cross over to a regime of algebraic decay driven by a delicate balance between surface tension and extensional viscosity. For all fluids, the breakup time decreases exponentially with the flow rate ratio (q), which is proportional to the outer viscous stress.

The exponential decay of filament thickness allows measurement of the *steady* extensional viscosities (η_e) of all fluids. We develop a simple model based on normal stress balance that allows for the estimation of η_e for all fluids in the flow-driven regime. The base case scenario is the viscous Newtonian fluid, which serves as a good check since it is known that, for a Newtonian fluid, $\eta_e = 3\eta_s$. Our estimates for the Newtonian fluids are in very close agreement with the theoretical values (figure 9). The values of extensional viscosity for the viscoelastic fluids show the expected qualitative features such as strain-rate hardening. Also, the values of extensional viscosity decrease non-monotonically as polymer MW is decreased. The measured values of η_e for polymeric fluids deviate somewhat from the predicted FENE-P values, although the general trend is similar.

In addition, we report a new streaming regime (elastic tip-streaming) in which both surface tension and elastic stresses are at play. In this regime, very small droplets are ejected from the tip of the mother drop, which is similar to tip-streaming in surfactant laden Newtonian filament. However, due to elastic stresses, the mother-drop advances and recoils while ejecting the droplets. This regime is only found for high MW fluids and at large flow rate ratios.

In summary, it is shown that elastic stresses have a significant effect on the filament thinning and drop breakup process. The effects become more pronounced as the polymer MW is increased, even though the normalized concentration remains constant. Measurements show that the thinning process has all the features of a *steady* extensional flow and thus can be used to estimate the *steady* extensional viscosity values of various fluids.

Acknowledgments

We thank Anke Lindner, Alexander Morozov, Christian Wagner and Michael Graham for fruitful discussions. This work was supported by the National Science Foundation through grants MRSEC/DMR05-20020 and CBET-0932449.

References

[1] Goldin M *et al* 1969 Breakup of laminar capillary jet of a viscoelastic fluid *J. Fluid Mech.* **38** 689
[2] Shi X D, Brenner M P and Nagel S R 1994 A cascade of structure in a drop falling from a faucet *Science* **265** 219–22
[3] Eggers J 1997 Nonlinear dynamics and breakup of free-surface flows *Rev. Mod. Phys.* **69** 865–929
[4] Eggers J 2005 Drop formation—an overview *Z. Fur Angew. Math. Mech.* **85** 400–10
[5] Doshi P *et al* 2003 Persistence of memory in drop breakup: The breakdown of universality *Science* **302** 1185–8
[6] Anna S L, Bontoux N and Stone H A 2003 Formation of dispersions using 'flow focusing' in microchannels *Appl. Phys. Lett.* **82** 364–6
[7] Dreyfus R, Tabeling P and Willaime H 2003 Ordered and disordered patterns in two-phase flows in microchannels *Phys. Rev. Lett.* **90** 144505
[8] Garstecki P, Stone H A and Whitesides G M 2005 Mechanism for flow-rate controlled breakup in confined geometries: a route to monodisperse emulsions *Phys. Rev. Lett.* **94** 164501
[9] Thorsen T *et al* 2001 Dynamic pattern formation in a vesicle-generating microfluidic device *Phys. Rev. Lett.* **86** 4163–6

[10] Utada A S *et al* 2005 Monodisperse double emulsions generated from a microcapillary device *Science* **308** 537–41
[11] Garstecki P *et al* 2004 Formation of monodisperse bubbles in a microfluidic flow-focusing device *Appl. Phys. Lett.* **85** 2649–51
[12] Gordillo J M *et al* 2004 A new device for generation of microbubbles *Phys. Fluids* **16** 2828–35
[13] Link D R *et al* 2004 Geometrically mediated breakup of drops in microfluidic devices *Phys. Rev. Lett.* **92** 054503
[14] Arratia P E, Gollub J P and Durian D J 2008 Polymeric filament thinning and breakup in microchannels *Phys. Rev.* E **77** 036309
[15] Husny J and Cooper-White J 2006 The effect of elasticity on drop creation in T-shaped microchannels *J. Non-Newton. Fluid Mech.* **137** 121–36
[16] Steinhaus B, Shen A Q and Sureshkumar R 2007 Dynamics of viscoelastic fluid filaments in microfluidic devices *Phys. Fluids* **19** 073103
[17] Amarouchene Y *et al* 2001 Inhibition of the finite-time singularity during droplet fission of a polymeric fluid *Phys. Rev. Lett.* **86** 3558–61
[18] Christiani Y and Walker L M 2001 Surface tension driven jet breakup on strain-hardening polymer solutions *J. Non-Newton. Fluid Mech.* **100** 9–26
[19] Mun R P, Byars J A and Boger D V 1998 The effects of polymer concentration and molecular weight on the breakup of laminar capillary jets *J. Non-Newton. Fluid Mech.* **74** 285–97
[20] Oliveira M S N, Yeh R and McKinley G H 2006 Iterated stretching, extensional rheology and formation of beads-on-a-string structures in polymer solutions *J. Non-Newton. Fluid Mech.* **137** 137–48
[21] Sostarecz M C and Belmonte A 2004 Beads-on-string phenomena in wormlike micellar fluids *Phys. Fluids* **16** 67–70
[22] Tirtaatmadja V, McKinley G H and Cooper-White J J 2006 Drop formation and breakup of low viscosity elastic fluids: Effects of molecular weight and concentration *Phys. Fluids* **18** 043101
[23] Wagner C *et al* 2005 Droplet detachment and satellite bead formation in viscoelastic fluids *Phys. Rev. Lett.* **95** 164504
[24] Clasen C *et al* 2006 The beads-on-string structure of viscoelastic threads *J. Fluid Mech.* **556** 283–308
[25] Oliveira M S N and McKinley G H 2005 Iterated stretching and multiple beads-on-a-string phenomena in dilute solutions of highly-extensible flexible polymers *Phys. Fluids* **17** 071704
[26] Entov V M and Hinch E J 1997 Effect of a spectrum of relaxation times on the capillary thinning of a filament of elastic liquid *J. Non-Newton. Fluid Mech.* **72** 31–53
[27] McKinley G H and Sridhar T 2002 Filament-stretching rheometry of complex fluids *Annu. Rev. Fluid Mech.* **34** 375–415
[28] Lindner A, Vermant J and Bonn D 2003 How to obtain the elongational viscosity of dilute polymer solutions? *Physica* A **319** 125–33
[29] Anna S L and McKinley G H 2001 Elasto-capillary thinning and breakup of model elastic liquids *J. Rheol.* **45** 115–38
[30] Quake S R and Scherer A 2000 From micro- to nanofabrication with soft materials *Science* **290** 1536–40
[31] Sia S K and Whitesides G M 2003 Microfluidic devices fabricated in poly(dimetylsiloxane) for biological studies *Electrophoresis* **24** 3563–76
[32] Bird R B *et al* 1987 Dynamics of Polymeric Liquids: Fluid Mechanics vol 1, 2nd edn (New York: Wiley)
[33] Larson R G 1999 The rheology and structure of complex fluids (New York: Oxford University Press)
[34] Stoltz C, de Pablo J J and Graham M D 2006 Concetration dependence of shear and extensional rheology of polymer solutions: Brownian dynamics simulations *J. Rheol.* **50** 137–67
[35] Boger D V 1977 Highly elastic constant-viscosity fluid *J. Non-Newton. Fluid Mech.* **3** 87–91
[36] Boger D V 1987 Viscoelastic flows through contractions *Annu. Rev. Fluid Mech.* **19** 157–82
[37] Peterlin A 1966 Hydrodynamics of macromolecules in a velocity field with longitudinal gradient *J. Polym. Sci. Polym. Lett.* **4** 287–91

[38] Spiegelberg S H and McKinley G H 1996 Stress relaxation and elastic decohesion of viscoelastic polymer solutions in extensional flow *J. Non-Newton. Fluid Mech.* **67** 49–76
[39] Chang H C, Demekhin E A and Kalaidin E 1999 Iterated stretching of viscoelastic jets *Phys. Fluids* **11** 1717–37
[40] Jensen M J, Stone H A and Bruus H 2006 A numerical study of two-phase Stokes flow in an axisymmetric flow-focusing device *Phys. Fluids* **18** 077103
[41] Zhang D F and Stone H A 1997 Drop formation in viscous flows at a vertical capillary tube *Phys. Fluids* **9** 2234–42
[42] Zhou C F, Yue P T and Feng J J 2006 Formation of simple and compound drops in microfluidic devices *Phys. Fluids* **18** 092105
[43] Trouton F T 1906 On the coefficient of viscous traction and its relation to that of viscosity *Proc. R. Soc.* A **77** 426–40
[44] Arratia P E *et al* 2006 Elastic instabilities of polymer solutions in cross-channel flow *Phys. Rev. Lett.* **96** 144502
[45] Cohen I *et al* 1999 Two fluid drop snap-off problem: experiments and theory *Phys. Rev. Lett.* **83** 1147–50
[46] Lister J R and Stone H A 1998 Capillary breakup of a viscous thread surrounded by another fluid *Phys. Fluids* **10** 2758–64
[47] Fontelos M A and Li J 2004 On the evolution and rupture of filaments in Giesekus and FENE models *J. Non-Newton. Fluid Mech.* **118** 1–16
[48] Eggers J and Villermaux E 2008 Physics of liquid jets *Rep. Prog. Phys.* **71** 036601
[49] van Heel A P G, Hulsen M A and van den Brule B H A A 1998 On the selection of parameters in the FENE-P model *J. Non-Newton. Fluid Mech.* **75** 253–71